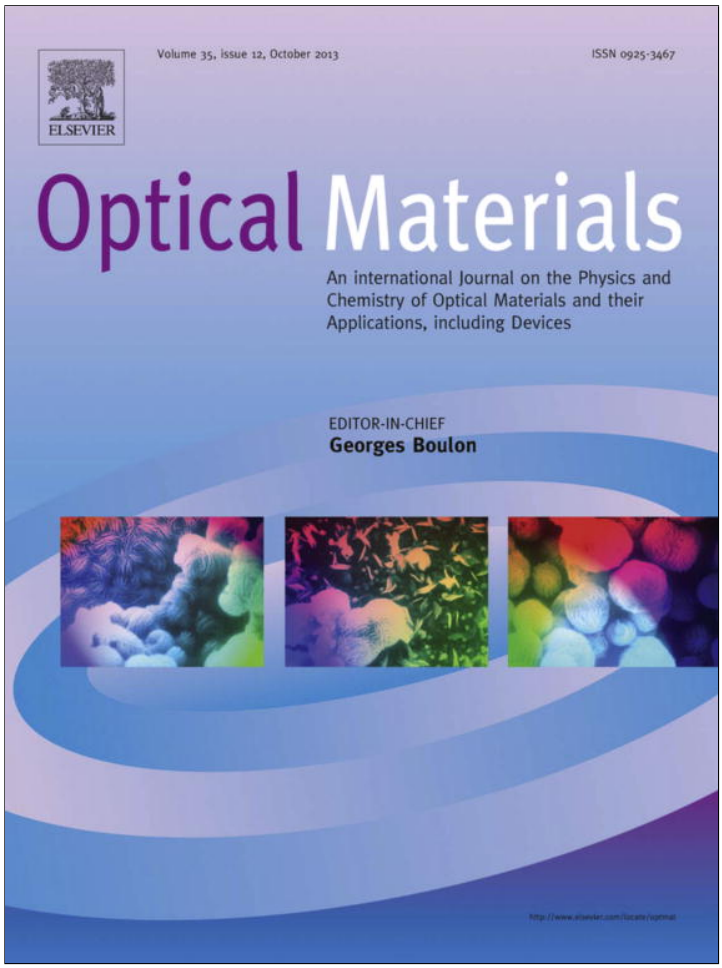

Optical Materials 35 (2013) 2261–2266

Contents lists available at SciVerse ScienceDirect

Optical Materials

journal homepage: www.elsevier.com/locate/optmat

Luminescence properties of $Na_3SrB_5O_{10}:Dy^{3+}$ plate-like microstructures for solid state lighting applications

G.R. Dillip [a], S.J. Dhoble [b], B. Deva Prasad Raju [c,a,*]

[a] Department of Physics, Sri Venkateswara University, Tirupati 517 502, India
[b] Department of Physics, RTM Nagpur University, Nagpur 440 033, India
[c] Department of Future Studies, Sri Venkateswara University, Tirupati 517 502, India

ARTICLE INFO

Article history:
Received 10 February 2013
Received in revised form 27 April 2013
Accepted 5 June 2013
Available online 29 June 2013

Keywords:
Inorganic phosphor
White light emitting diode (W-LED)
FE-SEM
Decay curves

ABSTRACT

A series of novel plate-like microstructure $Na_3SrB_5O_{10}$ doped with various Dy^{3+} ions concentration have been synthesized for the first time by solid-state reaction (SSR) method. X-ray diffraction (XRD) results demonstrated that the prepared $Na_3SrB_5O_{10}:Dy^{3+}$ phosphors are single-phase pentaborates with triclinic structure. The plate-like morphology of the phosphor is examined by Field emission scanning electron microscopy (FE-SEM). The existence of both BO_3 and BO_4 groups in $Na_3SrB_5O_{10}:Dy^{3+}$ phosphors are identified by Fourier transform infrared (FT-IR) spectroscopy. Upon excitation at 385 nm, the PL spectra mainly comprising of two broad bands: one is a blue light emission (~486 nm) and another is a yellow light emission (~581 nm), originating from the transitions of $^4F_{9/2} \rightarrow {}^6H_{15/2}$ and $^4F_{9/2} \rightarrow {}^6H_{13/2}$ in $4f^9$ configuration of Dy^{3+} ions, respectively and the optimized dopant concentration is determined to be 3 at.%. Interestingly, the yellow-to-blue (Y/B) emission integrated intensity ratio is close to unity (0.99) for 3 at.% Dy^{3+} ions, suggesting that the phosphors are favor for white illumination. Moreover, the calculated Commission International de l'Eclairage (CIE) chromaticity coordinates of $Na_3SrB_5O_{10}:Dy^{3+}$ phosphors shows the values lie in white light region and the estimated CCT values are located in cool/day white light region.

1. Introduction

In recent years, a tremendous emphasis is being placed on solid state lighting (SSL) devices due to their ever-increasing demands for novel lighting sources with high luminous efficiency and high environment safety [1,2]. Rare-earth (RE) ions doped inorganic phosphors have received considerable attention because of their excellent luminescent properties and wide applications in SSL, optical filters, fluorescent lamps, field emission displays, solid-state lasers, etc. Within these, many researchers have been motivated to the development of SSL devices, which utilizes the white light emitting diodes (W-LEDs) [3,4]. In general, three dominant methods are used to produce a white light spectrum using LEDs. The first is packaging multiple LEDs into a single device that emit three primary colors (*Red*, *Green and Blue* (***RGB***)) and then mix to all the colors to generate a spectrum which is perceived white light by the human eye. Moreover, the directional nature of LED output makes this approach not suitable for general illumination application [5]. Another more practical method for producing W-LEDs is to combine a single LED (*most often blue*) with phosphor(*s*) that will absorb a portion the higher energy light from the LED and emit a balancing color to produce white. However, the phosphors have fabricated by this method resulting to both a decrease in luminous efficiency due to re-absorption and poor reproducibility [6]. And other is use of near-UV (350–410 nm) LED chip mounted with tricolor (RGB) phosphors. But, in the three converter system, the blue emission efficiency is poor because of the strong re-absorption of the blue light by the red or green emitting phosphors [7]. Hence, the current lighting technology requires the single-phased white light emitting phosphors to overcome these short comings [8]. Thus, the researchers adapted an alternative way to achieve white light with high color rendering index (CRI) and suitable CCT that can generate warm/cool/day white light. Up to now, a few materials have been reported in literature to enhance the luminous efficiency and to reduce the energy crises [9,10]. Therefore, the search for novel rare-earth ions doped single-phased white light phosphor with perfect stability and color reproducibility for their use in near-UV pumped W-LEDs is obvious interest and importance.

Trivalent RE ions having 4*f*–4*f* inner-shell transitions possess specific advantages features, such as high luminescence yield, narrow emission line, and long decay time constant [2]. Thus, most rare-earth elements are often doped into many light emitting materials and laser materials. Currently, trivalent dysprosium ions

* Corresponding author at: Department of Future Studies, Sri Venkateswara University, Tirupati 517 502, India. Tel.: +91 9440281769.
E-mail address: drdevaprasadraju@gmail.com (B. Deva Prasad Raju).

0925-3467/$ - see front matter © 2013 Elsevier B.V. All rights reserved.
http://dx.doi.org/10.1016/j.optmat.2013.06.012

(Dy^{3+}) doped phosphors are of great interest because of its white light emission. Usually, Dy^{3+} ions have two dominant emission bands: one is in blue region (470–500 nm) due to $^4F_{9/2} \rightarrow {}^6H_{15/2}$ transition and other is in yellow region (570–600 nm) corresponding to the $^4F_{9/2} \rightarrow {}^6H_{13/2}$ transition [11]. More importantly, one of the dominant factors to achieve the white light is the yellow-to-blue (Y/B) luminescence integrated intensity ratio of Dy^{3+} ions, which is required to unity. Therefore, the resultant phosphor emits light in warm/cool/day light region, allowing for the utilization into a wide range of lighting applications. In general, the relative intensities of these two emission bands depend on the host composition, doping concentration and excitation wavelength [12]. The emission spectra of RE ions almost remain the same in different hosts, but the luminescent efficiency, chemical stability and durability depend on physical properties of the hosts selected [13]. In order to identify novel and potential phosphor materials for W-LEDs, selection of host material is significant.

Over the past, much effort has been devoted to the development of Dy^{3+} ions doped phosphorescence host matrices for white light emission, such as borates [14], phosphates [15], vanadates [16], molybdates [17], and silicates [18]. Owing to their unique physical and optical properties, the borates are considered as suitable and potential host matrices for optical applications (fluorescence materials, phosphors and display devices, etc.). In order to search for new and economical as well as high efficient phosphors, many researchers focus their interest on alkali–alkaline earth metal borates. Till date, many reports have been appeared on the luminescence investigations of RE doped alkali–alkaline earth metal borate phosphors [14,19,20]. For instance, $KSr_4(BO_3)_3$:Dy^{3+}, Tm^{3+} and Eu^{3+} [19] and $NaSrBO_3$:Ce^{3+} [20], etc. Due to the importance of white light phosphors, in the present communication, the authors have chosen $Na_3SrB_5O_{10}$ as a host matrix and trivalent RE ion, Dy^{3+} as a dopant to prepare the $Na_3SrB_5O_{10}$:Dy^{3+} phosphors via conventional SSR method to explore its suitability for W-LEDs. To the best of our knowledge, it is the first report on the photoluminescence properties of a novel $Na_3SrB_5O_{10}$:Dy^{3+} material. In addition, the authors are also presented the results of XRD, FTIR, FE-SEM, Energy dispersive X-ray spectroscopy (EDS) and decay curve measurements on $Na_3SrB_5O_{10}$:Dy^{3+} powders upon different Dy^{3+} dopant concentration.

2. Experimental section

2.1. Sample preparation

The series of samples investigated in this work is according to $Na_3Sr_{1-x}B_5O_{10}$:Dy^{3+}_x (x = 0, 1, 3, 5 and 7 at.%) molecular formula and were prepared using the conventional SSR method. The starting materials of analytical reagent (AR) grade Na_2CO_3, $SrCO_3$, H_3BO_3 and Dy_2O_3 were used as received in the preparation of phosphors without further purification. Firstly, the stoichiometric quantities of raw materials were calculated and then mixed homogeneously in an agate mortar for 1 h. Later, each of the samples were put into porcelain crucibles and gradually heated up to 800 °C in an electric furnace and kept at this temperature for 8 h. After sintering, the products were cooled down to room temperature (RT) inside the furnace itself and then the powders with white body color were obtained. The powders were further ground again into fine powder for experimental measurements.

2.2. Measurements

The structure of all prepared poly-crystalline powders were checked by a Rigaku Smartlab X-ray diffractometer with Cu Kα radiation (λ = 1.5406 Å) at 40 kV and 20 mA. The data for $Na_3SrB_5O_{10}$:Dy^{3+} (Dy^{3+} = 0, 1, 3, 5 and 7 at.%) were collected over a 2θ range between 10° and 80° with a step size of 0.02°. FTIR spectra were recorded with a Bruker Alpha-T FT-IR spectrophotometer with KBr pellet technique in the spectral range from 4000 to 500 cm^{-1}. The morphology of the sample was inspected with a field emission scanning electron microscopy (FE-SEM, ZEISS, Japan). The presence of elements in the prepared sample was confirmed by EDS analysis on the FE-SEM attached EDS instrument. Thermogravimetric analysis (TGA) and differential thermal analysis (DTA) was recorded on an EXSTAR 6000 Thermal analyzer at a heating rate of 10 °C/min under nitrogen atmosphere and the range was varied from RT to 700 °C. UV–Vis diffuse reflectance spectra (DRS) were measured on a UV–Vis spectrophotometer (Jasco, Japan) using $BaSO_4$ as a standard measurement. Photoluminescence (PL) and excitation (PLE) spectra were recorded using a fluorescent spectrophotometer (Jobin Vyon Fluorolog–3 fluorometer) with a Xenon lamp as the excitation source and the luminescence decay curves were also recorded on the same instrument. For PL, PLE and decay curve measurements, the samples were taken in pellet form and all the measurements were carried out at RT.

3. Results and discussion

3.1. XRD studies

In order to confirm the structure and phase purity of the prepared samples, the powder XRD analysis was carried out. The comparison of powder XRD patterns of $Na_3SrB_5O_{10}$:Dy^{3+} (Dy^{3+} = 0, 1, 3, 5 and 7 at.%) phosphors are shown in Fig. 1. All the observed peaks made for $Na_3SrB_5O_{10}$:Dy^{3+} phosphors are found to be comparable with those reported in the inorganic crystal structure database (COD ID No: 2016662). It is noticed from the patterns that there are no Dy_2O_3 peaks in the diffractogram indicating that the introduced activator, Dy^{3+} ions are incorporated into the $Na_3SrB_5O_{10}$ host lattices. Recently, Wu et al. [21], solved, the single crystal structure of a novel alkali–alkaline earth pentaborate $Na_3SrB_5O_{10}$ by the refinement of single crystal XRD data using full-matrix least squares technique, which revealed a triclinic crystal structure with space group $P\bar{1}$ and the cell parameters are a = 7.277 (2) Å, b = 7.601 (2) Å, c = 9.728 (2) Å, α = 81.062 (16)°, β = 71.538 (15)°, γ = 61.636 (15)° and Volume = 446.43 (19) $Å^3$. According to Wu et al. [21], the basic structural unit of $Na_3SrB_5O_{10}$ is the $[B_5O_{10}]^{5-}$ group that composed of four $[BO_3]$ triangles (Δ) and one $[BO_4]$ tetrahedron (□) and the $[B_5O_{10}]^{5-}$ groups are not directly linked to each other but connected via SrO_8 and NaO_n (n = 6 or 7) ployhedra, forming a complex three-dimensional array. Further, the possible sites for incorporating Dy^{3+} ions in

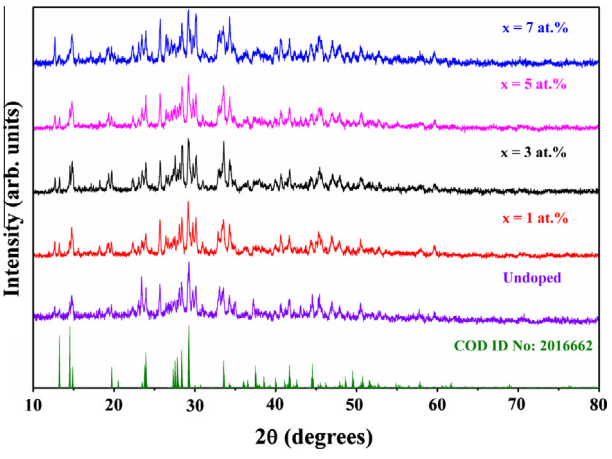

Fig. 1. XRD patterns of $Na_3Sr_{1-x}B_5O_{10}$:Dy^{3+}_x (x = 0–7 at.%) phosphors.

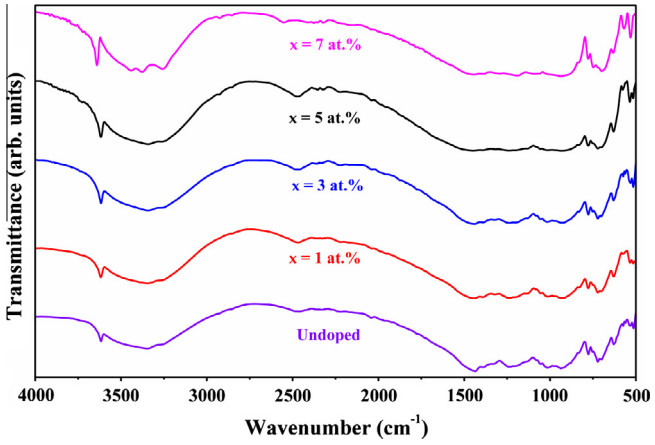

Fig. 2. FTIR spectra of $Na_3Sr_{1-x}B_5O_{10}:Dy_x^{3+}$ (x = 0–7 at.%) phosphors.

$Na_3SrB_5O_{10}$ phosphors are the $Na^+/Sr^{2+}/B^{3+}$ cation sites. The ionic radii for 8-coordinated Sr^{2+} and Dy^{3+} are 1.26 and 1.03 Å, respectively [22,23]. However, the ionic radius for 6-coordinated Na^+ is 0.39 Å [20] and that for 4-coordinated B^{3+} is 0.11 Å [22]. On basis of the disparity of ionic sizes and the differential valence states among $B^{3+}/Dy^{3+}/Sr^{2+}/Na^+$, we predicted that Dy^{3+} would occupy the Sr^{2+} position instead of B^{3+}/Na^+ sites in the host structure. In accordance with the ionic size variation between Sr^{2+} and Dy^{3+} ions, the substitution of Dy^{3+} ions at Sr^{2+} cation sites resulted in the shifting of diffraction peaks to higher angle region with increasing of Dy^{3+} ions concentration. Hence, the authors believed that the charge loss is most probably compensated by Sr^{2+} vacancies (V_{Sr}) followed by, $3Sr^{2+} \rightarrow 2Dy^{3+} + V_{Sr}$.

3.2. FTIR studies

To further substantiate the coordination surrounding of B–O in the $Na_3SrB_5O_{10}:Dy^{3+}$ (Dy^{3+} = 0, 1, 3, 5 and 7 at.%) phosphors, the FTIR spectra were recorded and are depicted in Fig. 2. The assignment of vibrations for all samples was similar in nature and there is no significant peak shifting is observed. It can be seen from the spectra that the strong bands appeared in the range from 1202 and 1435 cm^{-1} should be assigned as the BO_3 asymmetric stretching vibrations and those between 923 and 1055 cm^{-1} are mainly attributed to BO_4 asymmetric stretching modes. The bands associated with BO_3 and BO_4 out of plane bending modes are overlapped and located at about 774 cm^{-1} [24]. Bands with the frequencies below 550 cm^{-1} might be due to the Na–O and Sr–O vibrations [25]. The strong broad absorption band and a sharp absorption peak located at about 3344 and 3617 cm^{-1}, respectively are clearly indicated the presence of –OH group in the samples, which is the characteristic vibrations of water from air, physically absorbed on the sample surface [15]. Further, the above results confirmed the existence of both triagonally and tetrahedrally coordinated boron atoms in the prepared phosphors, which are in agreement with those compounds containing BO_3 and BO_4 groups in literature [24–26].

3.3. FE-SEM and EDS analysis

To investigate the morphology of the sample, the FE-SEM images were recorded. A typical low magnification FE-SEM image of $Na_3SrB_5O_{10}:Dy^{3+}$ (Dy^{3+} = 3 at.%) phosphor is shown in Fig. 3a. It is observed from the image that the phosphor exhibits plate-like morphology. In general, to improve the luminescence performance of the practical devices, the phosphor with regular morphology and fine size is essential. But, usually, the morphology of the resultant phosphors depends on the morphology of the starting materials, the sintering temperature, reaction duration and the process of grinding, etc. [2]. A typical high magnification FE-SEM image is shown in Fig. 3b. On careful observation, the average sizes of the phosphors might be in micrometer dimension. Hence, it could be suitable for fabricating the SSL devices. To further inspect the presence of dysprosium element in $Na_3SrB_5O_{10}:Dy^{3+}$ phosphors, the EDS analysis was carried out. A representative EDS spectrum of

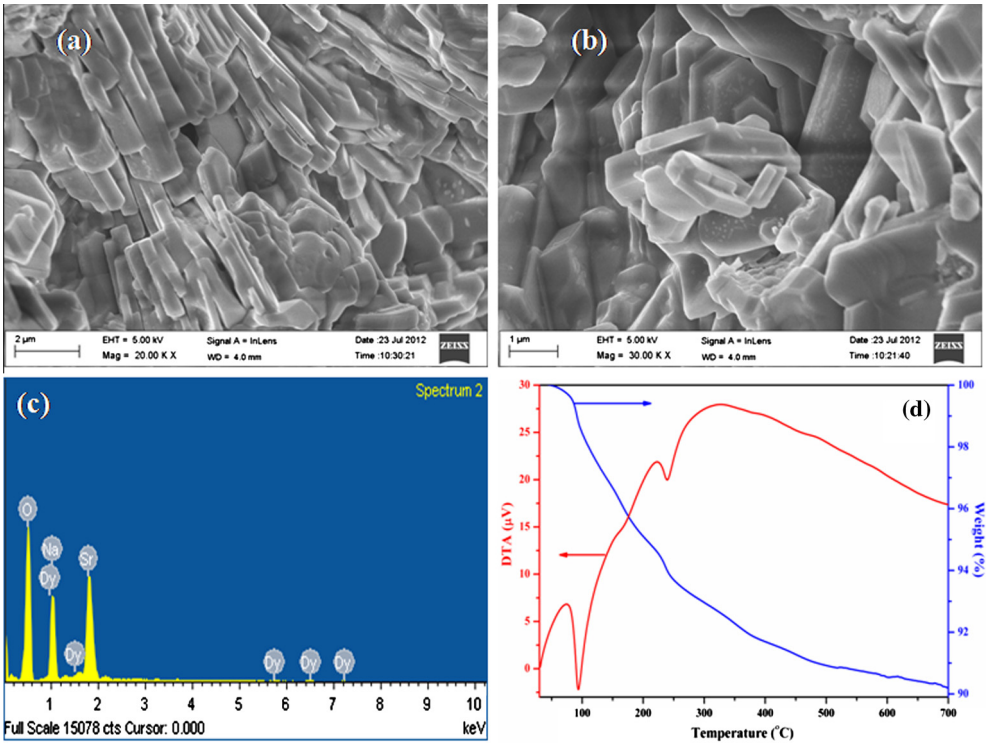

Fig. 3. (a) low-magnification and (b) high magnification FE-SEM images, (c) EDS profile and (d) TGA/DTA trace of $Na_3SrB_5O_{10}:Dy^{3+}$ (Dy^{3+} = 3 at.%) phosphors.

$Na_3SrB_5O_{10}:Dy^{3+}$ (Dy^{3+} = 3 at.%) phosphor is depicted in Fig. 3c, confirmed the presence of dopant (Dy) in $Na_3SrB_5O_{10}:Dy^{3+}$ phosphor. The absence of other impurity elements in EDS profile evidenced the phase purity of the obtained phosphor, consistent with structural analyses.

3.4. TGA/DTA analysis

In order to study the thermal properties of phosphor $Na_3SrB_5O_{10}:Dy^{3+}$, the TGA/DTA studies are carried out. Fig. 3d presents the TGA/DTA trace of the synthesized phosphor $Na_3SrB_5O_{10}:Dy^{3+}$ (Dy^{3+} = 3 at.%). The TGA curve shows two main stages of weight loss. The initial loss is observed in the range between 80 and 110 °C and the final loss from 215 to 350 °C might be due to the evaporation of absorbed moisture present on the surface of sample during the grinding process, which are confirmed by the appearance of endothermic peaks at about 95 °C and 240 °C and an exothermic peak appeared at ~325 °C, respectively in the DTA curve and also supporting the FTIR results [9,15]. No other significant weight loss is noticed in the TGA curve beyond this temperature and up to 700 °C.

3.5. DRS studies

Fig. 4 shows the DRS of phosphor $Na_3SrB_5O_{10}:Dy^{3+}$ (Dy^{3+} = 0, 1, 3, 5 and 7 at.%). In DRS, the host material shows a platform of high reflectance between 800 and 400 nm and then start to decrease from 400 to 200 nm. It is clear from the spectra that there is no detectable absorption is regarded in the entire region between 200 and 800 nm. When the Dy^{3+} ions were introduced into the host lattices of $Na_3SrB_5O_{10}$, Dy^{3+} doped phosphor $Na_3SrB_5O_{10}$ showed several absorption lines located at about 349, 364, 385 and 448 nm corresponding to $^6H_{15/2} \rightarrow {}^6P_{7/2}$, $^6H_{15/2} \rightarrow {}^6P_{5/2}$, $^6H_{15/2} \rightarrow {}^4I_{13/2}$ and $^6H_{15/2} \rightarrow {}^4I_{15/2}$, respectively [18]. These absorption lines are found to be consistent with those major excitation bands obtained from the excitation spectra (Fig. 5). Thus, the above results suggest that the introduction of rare earth ion, Dy^{3+} into the $Na_3SrB_5O_{10}$ host enhances the optical absorption in the near-UV region.

3.6. PL studies

Fig. 5 shows the excitation spectra of $Na_3SrB_5O_{10}:Dy^{3+}$ (Dy^{3+} = 1, 3, 5 and 7 at.%) phosphors with emission monitored at 486 nm

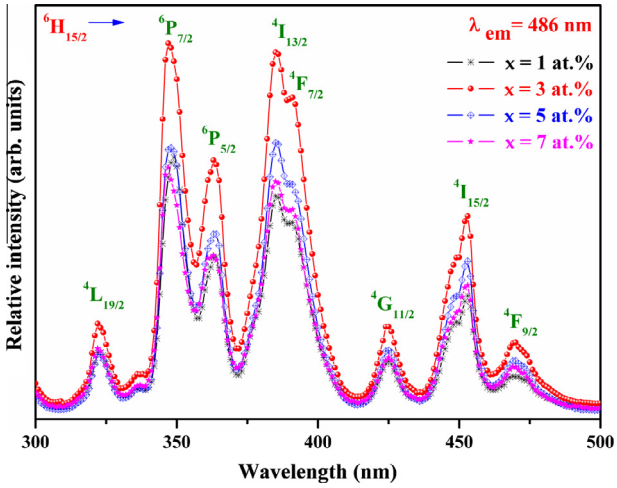

Fig. 5. Excitation spectra of $Na_3Sr_{1-x}B_5O_{10}:Dy_x^{3+}$ (x = 1–7 at.%) phosphors.

corresponding to the $^4F_{9/2} \rightarrow {}^6H_{15/2}$ transition of Dy^{3+} ions. In the wavelength range from 320 to 480 nm, the excitation spectra composed of several sharp lines located at about 322, 348, 363, 385 and 391, 425, 453 and 469 nm corresponds to the *f–f* transitions of Dy^{3+} ions from ground state $^6H_{15/2}$ to the various excited levels $^4L_{19/2}$, $^6P_{7/2}$, $^6P_{5/2}$, $^4I_{13/2}$+$^4F_{7/2}$, $^4G_{11/2}$, $^4I_{15/2}$ and $^4F_{9/2}$, respectively [27]. It can be noticed from the figure that the position and their regular pattern of every curve is very similar except for the intensity. The intensity of excitation peak was achieved highest for 3 at.% Dy^{3+} ions. Among the several absorption lines, the bands at around 348 and 385 nm are nearly equal intensity bands. However, on careful observation, the full width at half maximum (FWHM) of the peak at ~385 nm ($^6H_{15/2} \rightarrow {}^4I_{13/2}$) is greater than that of the band at ~348 nm ($^6H_{15/2} \rightarrow {}^4I_{13/2}$). Hence, the authors used 385 nm as an excitation wavelength to record the emission spectra of $Na_3SrB_5O_{10}:Dy^{3+}$ (Dy^{3+} = 1, 3, 5 and 7 at.%) phosphors. The strong excitation bands located in the wavelength region 350–410 nm imply that this kind of phosphor may have potential applications in the field of near-UV excited W-LEDs.

The emission spectra of $Na_3SrB_5O_{10}:Dy^{3+}$ (Dy^{3+} = 1, 3, 5 and 7 at.%) phosphors excited at 385 nm were depicted in Fig. 6. For all samples, the emission spectra are similar in nature except for the intensity and comprising of two main bands: one is in blue

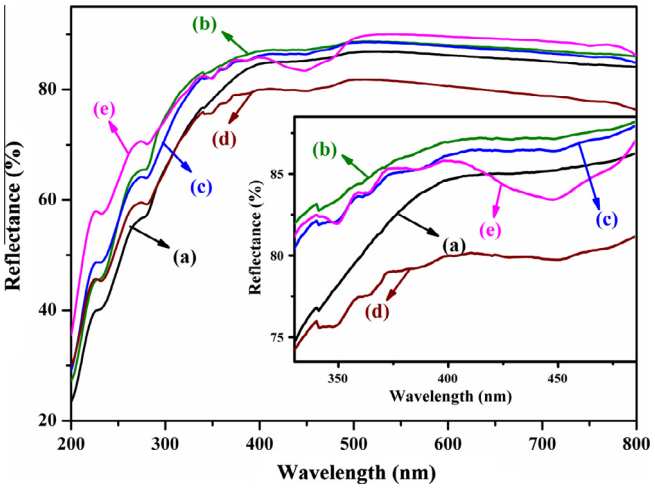

Fig. 4. UV–Vis diffuse reflectance spectra of $Na_3Sr_{1-x}B_5O_{10}:Dy_x^{3+}$ (x = *a*–*e* = 0–7 at.%) phosphors.

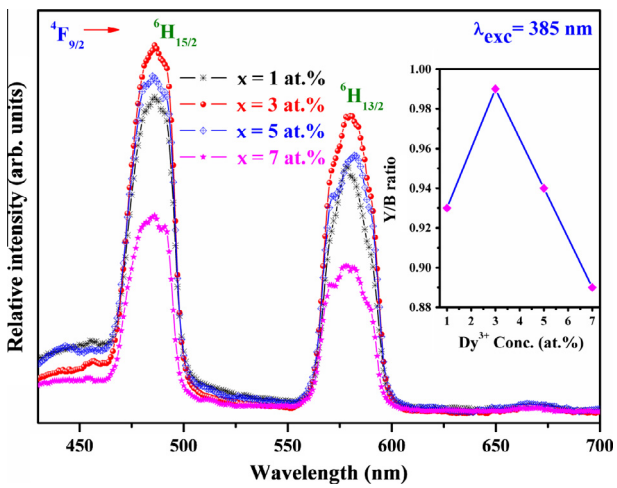

Fig. 6. Emission spectra of $Na_3Sr_{1-x}B_5O_{10}:Dy_x^{3+}$ (x = 1–7 at.%) phosphors. Inset shows the Y/B ratio with different Dy^{3+} ions concentration.

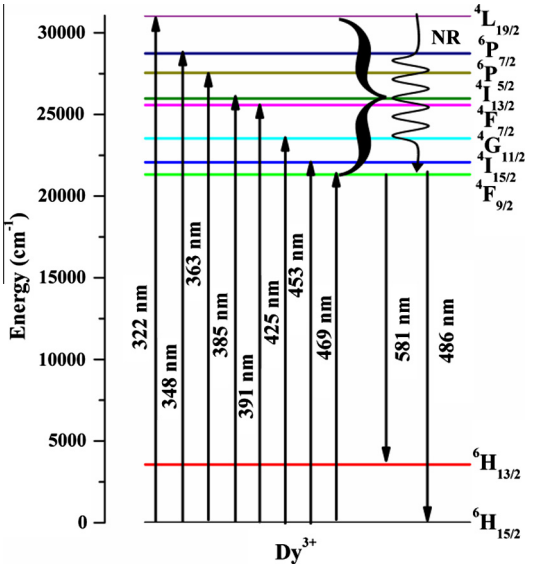

Fig. 7. A schematic energy level diagram of Dy^{3+} ions in $Na_3SrB_5O_{10}$ phosphors.

region (470–500 nm) and another in yellow region (570–600 nm). These two regions are the characteristic emissions of Dy^{3+} ions assigned to the transitions of $^4F_{9/2} \rightarrow {}^6H_{15/2}$ and $^4F_{9/2} \rightarrow {}^6H_{13/2}$, respectively. Fig. 7 represents the energy level scheme of Dy^{3+} ions in $Na_3SrB_5O_{10}$ phosphor. Well known to all that the $^4F_{9/2} \rightarrow {}^6H_{15/2}$ transition is chiefly magnetic dipole (MD) transition, which is hardly varies with the crystal field strength around Dy^{3+} ions, while the $^4F_{9/2} \rightarrow {}^6H_{13/2}$ transition belongs to a hypersensitive transition ($\Delta L = 2$ and $\Delta J = 2$), which is forced electric dipole (ED) transition and is strongly influenced by the chemical environment surrounding to Dy^{3+} ions [6]. It is clear from the spectra that the emission at ~486 nm corresponds to the transition $^4F_{9/2} \rightarrow {}^6H_{15/2}$ is predominant in $Na_3SrB_5O_{10}$:Dy^{3+}, suggesting that the Dy^{3+} ions occupy the site with high inversion symmetry. In addition, the integrated intensity ratio between the two transitions is a measure of the site symmetry where the Dy^{3+} ions are situated [28]. The calculated Y/B ratios are presented in Table 1. Further, to find the critical concentration of Dy^{3+} ions, the dopant concentration is varied between 1 and 7 at.% with the intervals of 2 at.%. With the increase of Dy^{3+} ions concentration, firstly, the intensity of both blue and yellow emissions are increased and then reached maximum extent at 3 at.%, then decreased with further increase of Dy^{3+} ions concentration due to concentration quenching of Dy^{3+} emission. The inset of Fig. 6 shows the variation of Y/B ratio with different Dy^{3+} ion concentration. It can be seen from the figure that the Y/B ratio increased with increasing of Dy^{3+} ion concentration from 0.93 to 0.99 and decreased further increase of dopant concentration. In many inorganic materials, an excessive doping of emission ions usually decreases the emission intensity remarkably because of the fact that the strong interaction occurs between activating ions with reduced distance, resulting a concentration quenching [29]. Due to the non-radiative energy transfer between dopant ions, the emission intensity decreased for 5 at.% Dy^{3+} ions. The concentration quenching may occur because the excitation energy migrates about a large number of centers before being emitted. With the increase of Dy^{3+} ions concentration, the average distance between Dy^{3+} ions will decrease. The excitation energy may transfer between the close Dy^{3+} ions by the exchange interaction. For this reason, it is necessary to obtain the critical distance (R_c) that is the critical separation between donors (activators) and acceptors (quenching site). The critical distance of the energy transfer R_c between the same activators, Dy^{3+} ions in the $Na_3SrB_5O_{10}$ phosphors can be estimated by the following formula suggested by Blasse [30]: $R_c = 2\left(\frac{3V}{4\pi X_c N}\right)^{1/3}$ where V is the volume of the unit cell, X_c is the critical concentration of the activator ion and N is the number of host cations (Sr^{2+}) in the unit cell. A rough estimate of the critical distance of energy transfer R_c was calculated by adopting the values of V, X_c and N as 446.43 Å^3, 0.03 and 2, respectively. Therefore, the critical transfer distance of Dy^{3+} ions in $Na_3SrB_5O_{10}$ phosphors is found to be ~24 Å. In addition, concentration quenching usually occurs as a result of non-radiative energy transfer among luminescent centers. Non-radiative energy transfer from one Dy^{3+} ion to another Dy^{3+} ion may occur by exchange interaction, radiation re-absorption or multipole–multipole interaction [10]. From the above results, it is concluded that the energy transfer between Dy^{3+} ions in the $Na_3SrB_5O_{10}$ phosphor are mainly magnetic dipole–dipole interactions.

Table 1
Variation of Y/B ratio, lifetimes and CCT values with the Dy^{3+} ions content in $Na_3SrB_5O_{10}$ phosphors.

Nominal Dy^{3+} contentin host (at.%)	Y/B ratio	Lifetimes τ (ms)	CCT values (~K)
1	0.93	0.78	7860
3	0.99	0.59	6193
5	0.94	0.58	7030
7	0.89	0.57	7080

3.7. Decay curve measurements

In order to explain the concentration quenching in more detail, the decay curve measurements of $Na_3SrB_5O_{10}$:Dy^{3+} (Dy^{3+} = 1, 3, 5 and 7 at.%) phosphors were performed. Fig. 8 shows the luminescence decay curves for $^4F_{9/2} \rightarrow {}^6H_{15/2}$ (486 nm) emission of $Na_3SrB_5O_{10}$:Dy^{3+} phosphor when excited with 385 nm. All the decay curves were well fitted by a second order exponential function, which is expressed as, $I(t) = A_1 \exp(-t/\tau_1) + A_2 \exp(-t/\tau_2)$, where A_1 and A_2 are the fitting parameters, τ_1 and τ_2 are the lifetimes. The average lifetimes could be calculated using the equation, $\tau = (A_1\tau_1^2 + A_2\tau_2^2)/(A_1\tau_1 + A_2\tau_2)$ [31]. The calculated lifetime values are presented in Table 1. With the increase of Dy^{3+} ions concentration, the lifetimes decreased due to fact that both the energy transfer rate between Dy^{3+}–Dy^{3+} and the probability of energy transfer to luminescent killer sites (such as defects) increased. The observed decay curve investigations are also supporting that the concentration quenching occurs in the $Na_3SrB_5O_{10}$:Dy^{3+} (Dy^{3+} = 1, 3, 5 and 7 at.%) phosphor [2].

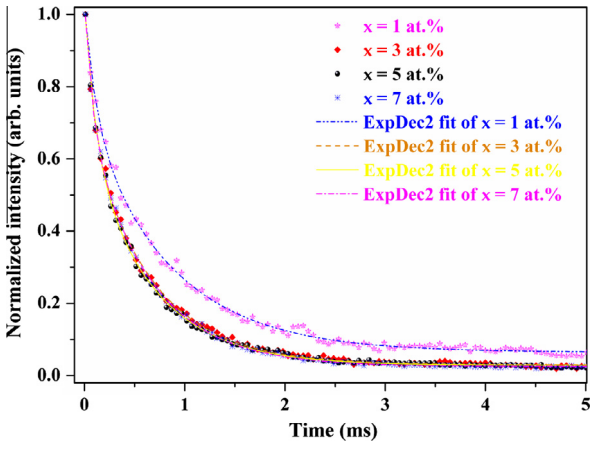

Fig. 8. Luminescence decays of $Na_3Sr_{1-x}B_5O_{10}$:Dy^{3+}_x (x = 1–7 at.%) phosphors and the fitted curves with second order exponential decay function (excited at 385 nm and monitored at 486 nm).

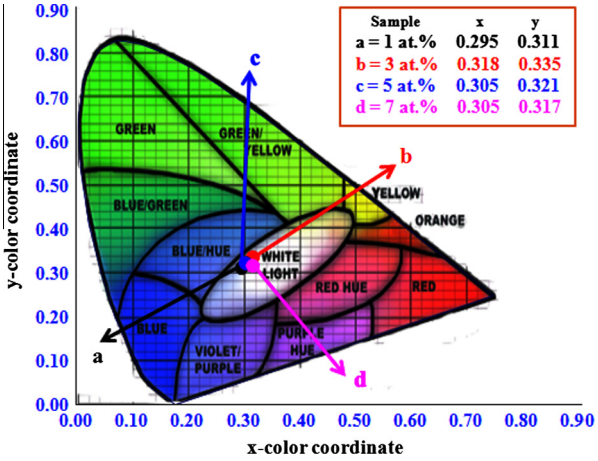

Fig. 9. CIE chromaticity coordinates of $Na_3Sr_{1-x}B_5O_{10}:Dy^{3+}_x$ ($x = a–d = 1–7$ at.%) phosphors.

3.8. CIE and CCT analysis

Usually, the potentiality of phosphors is examined by CIE chromaticity coordinates. Thus, to examine the applicability of the $Na_3SrB_5O_{10}:Dy^{3+}$ phosphors in W-LEDs, the CIE 1931 chromatic coordinates are calculated. In general, the color of any light source can be represented on the (x,y) coordinate in this color space [32]. The chromaticity coordinates for $Na_3SrB_5O_{10}:Dy^{3+}$ phosphors with different dopant contents are calculated using CIE calculates software from their corresponding emission spectra excited by 385 nm and are shown in Fig. 9. Well known to all that the CIE chromaticity coordinates are very similar, when the emission spectra profiles are identical [2]. In this figure, a, b, c and d represents the color coordinates for 1 (0.295, 0.311), 3 (0.318, 0.335), 5 (0.305, 0.321) and 7 (0.305, 0.317) at.% of Dy^{3+} ions in $Na_3SrB_5O_{10}:Dy^{3+}$ phosphors, respectively. The obtained y-chromaticity coordinate (0.335) is close to ideal white y-color coordinate (0.33), while the x-color coordinate value is (0.318) for 3 at.% Dy^{3+} ions. The obtained color coordinates all are located within white light region. In order to further examine the quality of white light, the color correlated temperature (CCT) values are calculated using McCany empirical formula and is expresses as, $CCT = -449n^3 + 3525n^2 - 6823n + 5520.33$, where $n = (x - x_e)/(y - y_e)$ is the inverse slope line, and $x_e = 0.332$ and $y_e = 0.186$ [33]. The estimated CCT values are located in day light region except for 3 at.% Dy^{3+} ions. The CCT value of 3 at.% Dy^{3+} is ~6193 K, which is close to cool white light region. Presently, the different countries people utilizing warm/cool/day light according to their preferences. For instance, in the USA, warm white (2800 K to 3000 K) is dominant for domestic applications. But in Japan, for example, 5000 K is dominant, in some other countries prefer even higher CCT up to 7500 K. Therefore, the manufacturers are considering a goal of realizing sun light spectra or daylight spectra with white LEDs zzbecause these are the most natural light that the human eyes have been adapted [34]. Hence, the synthesized phosphor might be applicable for the generation of cool/day white light emission excitable at UV (385 nm) LED in the field of SSL.

4. Conclusions

In summary, the above presented research has been focused on new $Na_3SrB_5O_{10}$ phosphors doped with Dy^{3+} ions, which were thermally treated at 800 °C in order to synthesize the phosphors via traditional SSR method. The dopant Dy^{3+} ions occupied the Sr^{2+} sites with high inversion symmetry in the host matrix. The phosphor has plate-like shapes, which are in micrometer dimension. Upon 385 nm excitation, the blue emission at ~486 nm ($^4F_{9/2} \rightarrow {}^6H_{15/2}$) and the yellow emission at ~581 nm ($^4F_{9/2} \rightarrow {}^6H_{13/2}$) have been observed and the $^4F_{9/2} \rightarrow {}^6H_{15/2}$ transition had highest intensity, indicating that the Dy^{3+} ions having high symmetry environment. The highest lifetimes of 0.78 ms was obtained at 1 at.% Dy^{3+} ions for this system. The evaluated CCT values are located in the cool/day white light region.

Acknowledgements

The authors are sincerely thankful to DRS facility extended by Dr. S. Kaleemulla, Assistant Professor in Physics, Materials Physics Division, School of Advanced Sciences, VIT University, Vellore.

References

[1] L. Zhang, H. Zhong, X. Li, L. Cheng, L. Yao, J. Sun, J. Zhang, R. Hua, B. Chen, Physica B 407 (2012) 68–72.
[2] L. Cheng, X. Li, L. Sun, H. Zhong, Y. Tian, J. Wan, W. Lu, Y. Zheng, T. Yu, L. Huang, H. Yu, B. Chen, Physica B 405 (2010) 4457–4461.
[3] Z. Xia, J. Zhuang, H. Liu, L. Liao, J. Phys. D: Appl. Phys. 45 (2012) 015302–015308.
[4] G.R. Dillip, S.J. Dhoble, L. Manoj, C.M. Reddy, B.D.P. Raju, J. Lumin. 132 (2012) 3072–3076.
[5] D.A. Steigerwald, J.C. Bhat, D. Collins, R.M. Fletcher, M.O. Holcomb, M.J. Ludowise, P.S. Martin, S.L. Rudaz, IEEE J. Sel. Top. Quant. 8 (2002) 310.
[6] X.Y. Sun, J.H. Zhang, X. Zhang, S.Z. Lu, X.J. Wang, J. Lumin. 122 (2007) 955–957.
[7] L. Li, W. Zi, G. Li, S. Lan, G. Ji, S. Gan, H. Zou, X. Xu, J. Solid State Chem. 191 (2012) 175–180.
[8] N. Guo, Y. Zheng, Y. Jai, H. Qiao, H. You, New J. Chem. 36 (2012) 168–172.
[9] X. Dong, X. Cui, Z. Fu, S. Zhou, S. Zhang, Z. Dai, Mater. Res. Bull. 47 (2012) 212–216.
[10] J.Y. Han, W.B. Im, G.Y. Lee, D.Y. Jeon, J. Mater. Chem. 22 (2012) 8793–8798.
[11] M.J. Xin, Y.C. Tao, C.Q. Qing, J. Lumin. 130 (2010) 1320–1323.
[12] S. Sailaja, S.J. Dhoble, B.S. Reddy, J. Mol. Struct. 1003 (2011) 115–120.
[13] V.R. Bandi, Y.T. Nien, I.G. Chen, J. Appl. Phys. 108 (2010) 023111–023114.
[14] C.H. Huang, T.M. Chen, J. Phys. Chem. C 115 (2011) 2349–2355.
[15] G.R. Dillip, B.D.P. Raju, J. Alloys Compd. 540 (2012) 67–74.
[16] G. Jia, C. Zhang, S. Ding, L. Wang, L. Lia, H. You, Cryst. Eng. Comm. 14 (2012) 573–578.
[17] A.K. Parchur, R.S. Ningthoujam, S.B. Rai, G.S. Okram, R.A. Singh, M. Tyagi, S.C. Gadkari, R. Tewari, R.K. Vatsa, Dalton Trans. 40 (2011) 7595–7601.
[18] J. Zhang, B. Chen, J. Sun, X. Li, L. Cheng, H. Zhing, J. Phys. D: Appl. Phys. 45 (2012) 325105–325110.
[19] L. Wu, Y. Zhang, M. Gui, P. Lu, L. Zhao, S. Tian, Y. Kong, J. Xu, J. Mater. Chem. 22 (2012) 6463–6470.
[20] W.R. Liu, C.H. Huang, C.P. Wu, Y.C. Chiu, Y.T. Yeha, T.M. Chen, J. Mater. Chem. 21 (2011) 6869–6874.
[21] L. Wu, G. Roth, K. Sparta, X. Chen, Acta Crystallogr. C64 (2008) i53–i56.
[22] W.B. Im, N.N. Fellows, S.P. DenBaars, R. Seshadri, Y.I. Kim, Chem. Mater. 21 (2009) 2957–2966.
[23] X. Li, L. Guan, M. Sun, H. Liu, Z. Yang, Q. Guo, G. Fu, J. Lumin. 131 (2011) 1022–1025.
[24] X. Chen, M. Li, X. Chang, H. Zang, W. Xiao, J. Solid State Chem. 180 (2007) 1658–1663.
[25] M. Zhang, S. Pan, J. Han, Z. Zhou, J. Solid State Chem. 184 (2011) 825–829.
[26] X. Chen, M. Li, J. Zuo, X. Chang, H. Zang, W. Xiao, Solid State Sci. 9 (2007) 678–685.
[27] W. Zhao, S. An, B. Fan, S. Lin, Y. Da, J. Lumin. 132 (2012) 953–956.
[28] H.G. Cai, W.Y. Hua, W.C. Fang, Z.J. Chi, Chin. Phys. B 18 (2009) 4532–4604.
[29] V.R. Bandi, B.K. Grandhe, H.J. Woo, K. Jang, D.S. Shin, S.S. Yi, J.H. Jeong, J. Alloys Compd. 538 (2012) 85–90.
[30] G. Blasse, J. Solid State Chem. 62 (1986) 207.
[31] A.K. Parchur, A.I. Prasad, A.A. Ansari, S.B. Rai, R.S. Ningthoujam, Dalton Trans. 41 (2012) 11032–11045.
[32] X. Song, H. He, R. Fu, D. Wang, X. Zhao, Z. Pan, J. Phys. D: Appl. Phys. 42 (2009) 065409–065414.
[33] A.K. Parchur, A.I. Prasad, S.B. Rai, R.S. Ningthoujam, Dalton Trans. 41 (2012) 13810–13814.
[34] Y. Ohno, Proc. SPIE, Bellingham, vol. 5530 (2004) pp. 88–98.